J. Wind Eng. Ind. Aerodyn. 97 (2009) 548–559

Contents lists available at ScienceDirect

Journal of Wind Engineering and Industrial Aerodynamics

journal homepage: www.elsevier.com/locate/jweia

Numerical study of aerodynamic characteristics of a square prism in a uniform flow

Shinichi Oka [a], Takeshi Ishihara [b,*]

[a] C&I, Inc., 7-6-7, Hikarigaoka, Nerima-ku, Tokyo 179-0072, Japan
[b] The University of Tokyo, 7-3-1, Hongou, Bunkyo-ku, Tokyo 113-8656, Japan

ARTICLE INFO

Article history:
Received 16 May 2008
Received in revised form
3 August 2009
Accepted 11 August 2009
Available online 11 September 2009

Keywords:
LES
Square prism
Aerodynamic coefficients
Power spectrum
Spanwise sensitivity

ABSTRACT

Aerodynamic characteristics of a square prism in a uniform flow for various angles of attack have been investigated using LES turbulence model. The results show that mean aerodynamic coefficients, surface pressures, and flow patterns for all angles of attack agree favorably with experiments. In addition, spanwise length of computational domain is found to slightly influence the mean aerodynamic coefficients whereas it shows strong impacts on fluctuating aerodynamic coefficients, which motivates a development of grid-independent estimation method for quantitative evaluations of fluctuations. The predicted power spectral densities for fluctuating aerodynamic coefficients are in good agreements with experiments in primary frequencies, which can be explained by the flow patterns. Strouhal numbers obtained from the simulations also agree well with experiments and acute change observed around 14° is successfully captured. Finally, a method for estimating grid-independent fluctuating aerodynamic coefficients is proposed by using a systematic elongation of spanwise length and is validated by the numerical tests.

1. Introduction

Aerodynamics of rectangular cylinders, typically used in tall buildings, handrails, pylons, and towers, is essential in evaluations of flow induced vibration and noise problems. Mean aerodynamic coefficients are important for gust response evaluation. Negative gradient of mean lift coefficients could cause negative damping resulting in galloping (Parkinson, 1971; Shimizu et al., 2004), and fluctuating lift coefficient is a key to an evaluation of flow induced noise problems (Lighthill, 1952; Curle, 1955; Kato et al., 1993).

Square prism is a typical cross section of rectangular cylinders, and numerous experimental studies have been carried out previously (Vickery, 1966; Otsuki et al., 1978; Ohya et al., 1980; Mizota and Okajima, 1981; Bearman and Obasaju, 1982; Igarash, 1984; Nishimura and Taniike, 2000). It is well known that flow patterns can be classified into two types, perfect separation type where angles of attack is less than 14° and reattachment type where angle of attack is larger than 14°. In the perfect separation type, negative gradient of lift coefficients is observed that could result in galloping phenomenon. On the other hand, in reattachment type flows, shear layer separating at the leading edge reattaches to the body that could cause a fluttering phenomenon. At angle of attack around 14°, reattachment occurs intermittently. It is well known that aerodynamic coefficients change drastically at this point, i.e. mean drag coefficient becomes minimum and magnitude of the lift coefficient reaches maximum. Minimum fluctuating coefficients and maximum Strouhal number are observed in the vicinity of 14° attack angle (Vickery, 1966; Mizota and Okajima, 1981). Nishimura and Taniike (2000) have shown that power spectral density of fluctuating aerodynamic coefficients vary with angles of attack in which primary frequencies are closely related to vortex shedding in the wake.

Recently, many numerical studies have been conducted (Tamura et al., 1990; Bosch and Rodi, 1998; Taylor and Vezza, 1999; Hayashi and Ohya, 2000; Shimada and Ishihara, 2001; Hirano et al., 2002). In order to predict flow induced vibrations and noise, a numerical approach should accurately predict the following key aerodynamic characteristics:

(1) Variation of mean aerodynamic coefficients and negative gradient of lift coefficient in the range of angles of attack smaller than 14°, which is the critical angles range.
(2) Fluctuating aerodynamic coefficients vary with angles of attack.
(3) Acute change of Strouhal number observed at angle of attack around 14° that is related to change in vortex shedding patterns, and normalized power spectral densities of fluctuating coefficients, which have close relationship with vortex formation in the wake.

* Corresponding author. Tel.: +81 358411145; fax: +81 358411147.
E-mail address: ishihara@bridge.t.u-tokyo.ac.jp (T. Ishihara).

0167-6105/$ - see front matter © 2009 Elsevier Ltd. All rights reserved.
doi:10.1016/j.jweia.2009.08.006

Among previous numerical studies, three major approaches may be classified as follows:

The first approach is based on URANS (unsteady Reynolds averaged Navier Stokes) model. Shimada and Ishihara (2001) presented 2D analyzes for various section ratio rectangle cylinders using $k-\varepsilon$ model in which predictions of mean aerodynamic coefficients and Strouhal numbers are in good agreement with experiments. For B/D ratio 1:1 where flow is categorized in the perfect separation type, fluctuating aerodynamic coefficients favorably agree with experiments, because periodic components of fluctuating aerodynamic forces generated by Karman vortex shedding are dominant in this type. However, for reattachment type, the predictions do not quantitatively match with the experiments, indicating that RANS models are not suitable for reattachment type flows, because RANS is incapable of capturing stochastic component of fluctuating pressure (Bosch and Rodi, 1998).

The second approach is DNS (direct numerical simulation). Tamura et al. (1990) has predicted variation of mean aerodynamic coefficients of a square prism with various angles of attack using DNS in which third order upwind scheme is adopted. Predictions of both mean drag and lift coefficients are reported in good agreement with the experiments, however, there is no information about the fluctuating aerodynamic components in this study. Hayashi and Ohya (2000) presented impact of spanwise length on fluctuating aerodynamic coefficients of 1:0.6 rectangle cylinder at 0° angle of attack, and found that accuracy of fluctuations can be improved by increasing spanwise length. This fact indicates that capturing three dimensionality of vortexes is important to obtain accurate prediction of fluctuating aerodynamic coefficients. Rodi (1997) has also indicated that spanwise length should be more than four times longer than edge length of the rectangle cylinder. A sufficient length of computational domain in spanwise direction is required for accurate predictions of fluctuating aerodynamic forces. However, use of large spanwise length requires huge amount of computational costs.

The third approach is LES (large eddy simulation) in which large eddies are directly resolved while subgrid size small eddies are modeled. The advantage of this turbulence model is that it addresses stochastic components of turbulence fluctuations, three dimensionality of vortex, and high Reynolds number flows. Hirano et al. (2002) conducted a numerical study of flow around 2:1 rectangular cylinder using LES. The predicted results were reported to have good agreement with the experiments for mean drag and lift coefficients as well as Strouhal number. However, fluctuating aerodynamic coefficients are not compared with an experiment.

In this study, mean and fluctuating aerodynamic characteristics of square prism in a uniform flow are investigated using LES model to shed light on the predictions of fluctuating aerodynamics. Section 2 describes the numerical model and boundary conditions used in the present study. Section 3 presents variation of mean aerodynamic coefficients, pressure coefficients, flow patterns, and relationships between them. Section 4 focuses on fluctuating aerodynamic coefficients, Strouhal number, and power spectral analysis for various angles of attacks. The relationship between flow patterns and primary frequencies of power spectral is presented. In Section 5, a method of predicting grid-independent fluctuating aerodynamic coefficients is proposed using systematic elongation of spanwise length, and is validated by the numerical tests. The cost performance of the proposed method is also analyzed.

2. Numerical model and boundary conditions

2.1. Governing equations

The governing equations employed in LES model are obtained by filtering the time-dependent Navier–Stokes equations as follows:

$$\frac{\partial \rho \tilde{u}_i}{\partial x_i} = 0 \tag{1}$$

$$\frac{\partial}{\partial t}(\rho \tilde{u}_i) + \frac{\partial}{\partial x_j}(\rho \tilde{u}_i \tilde{u}_j) = \frac{\partial}{\partial x_j}\left(\mu \frac{\partial \tilde{u}_i}{\partial x_j}\right) - \frac{\partial \tilde{P}}{\partial x_i} - \frac{\partial \tau_{ij}}{\partial x_j}, \tag{2}$$

where $\tilde{u}_j$ and $\tilde{p}$ are filtered mean velocity and filtered pressure respectively. ρ is density and τ_{ij} is subgrid-scale stress defined by:

$$\tau_{ij} \equiv \rho \overline{u_i u_j} - \rho \overline{u_i} \overline{u}_j \tag{3}$$

The subgrid-scale stresses resulting from the filtering operations are unknown, and modeled as follows:

$$\tau_{ij} = -2\mu_t \tilde{S}_{ij} + \tfrac{1}{3}\tau_{kk}\delta_{ij}, \tag{4}$$

where μ_t is subgrid-scale turbulent viscosity, and $\tilde{S}_{ij}$ is the rate-of-strain tensor for the resolved scale defined by:

$$\tilde{S}_{ij} \equiv \frac{1}{2}\left(\frac{\partial \tilde{u}_i}{\partial x_j} + \frac{\partial \tilde{u}_j}{\partial x_i}\right). \tag{5}$$

2.2. Smagorinsky model

Smagorinsky model (Smagorinsky, 1963) is used for the subgrid-scale turbulent viscosity, μ_t.

$$\mu_t = \rho L_s^2 |\tilde{S}| = \rho L_s \sqrt{2\tilde{S}_{ij}\tilde{S}_{ij}}, \tag{6}$$

where L_s is the mixing length for subgrid-scales, and defined as:

$$L_s = \min(\kappa\delta, C_s V^{1/3}). \tag{7}$$

where κ is the von Karman constant, 0.42, C_s is Smagorinsky constant, δ is the distance to the closest wall, and V is the volume of a computational cell.

In general, $C_s = 0.1$ is widely used in the simulation by finite volume/difference methods. Most of them employed explicit discritization scheme for unsteady term in which negative numerical diffusions are inherently contained. On the other hand, no numerical diffusion schemes such as spectral method use small value for C_s. In this study, the second order implicit discritization scheme is utilized, in which numerical diffusions are small and positive. In order to determine C_s used in this study, systematic study was conducted for the flow around a circular cylinder in advance. The aerodynamic coefficients obtained by using C_s of 0.032 are closest to those by the spectral method (Ma et al., 2000).

2.3. Boundary conditions

When a wall-adjacent cell is in the laminar sublayer, the wall shear stress is obtained from the laminar stress–strain relationship as follows:

$$\frac{\tilde{u}}{u_\tau} = \frac{\rho u_\tau y}{\mu}, \tag{8}$$

If the mesh cannot resolve the laminar sublayer, it is assumed that the centroid of the wall-adjacent cells falls within the logarithmic region of the boundary layer, and the law-of-the-wall is employed.

$$\frac{\tilde{u}}{u\tau_\tau} = \frac{1}{\kappa}\ln E\left(\frac{\rho u_\tau y}{\mu}\right) \tag{9}$$

where $\tilde{u}$ is filtered velocity that is tangential to the wall, u_τ is friction velocity, κ is von Kármán constant, and constant E is 9.8. Uniform velocity condition is specified at inlet boundary, and zero diffusive conditions is used at the outlet boundary. Symmetry conditions are given for both sides and upper/lower boundaries.

2.4. Numerical method

Finite volume method and unstructured collocated mesh are used for the present simulations. The second order central difference scheme is used for the convective and viscosity term, and the second order implicit scheme for the unsteady term. SIMPLE (semi-implicit pressure linked equations) algorithm is employed for solving the discritized equations (Ferziger and Peric, 2002).

2.5. Modeling conditions and system configurations

Fig. 1 shows a computational domain and mesh used in the present study. The computational domain is square as shown in Fig. 1(a), and length of each side of the domain is 60*D*. Mesh density is higher at the corners and total 62 grids are distributed in an edge as shown in Fig. 1(b). LES requires a uniform grid in theory. However, it is impossible for the simulation of boundary layer and non-uniform grids are widely used in practice. A systematic study by changing aspect ratio of grid size in the vicinity of the square prism was conducted and it was noticed that the present non-uniform mesh does not affect the results. The corners of the square prism are rounded, as shown in Fig. 1(c), such that the radius of curvature is $D/100$ after Tamura et al. (1990). Each mesh size is $D/10$ in the spanwise direction. Uniform velocity, $U = 15$ m/s, is specified at flow inlet boundary condition, an edge length, D, of the square prism is 1 cm.

Parameters used in this study are shown in Table 1. The 12 angles of attack cases, 0°, 2°, 6°, 8°, 12°, 13°, 14°, 16°, 20°, 30°, and 45°, were simulated with 1*D* spanwise length model, and representative four angles of attack, 0°, 14°, 20°, and 45°, were performed with 6*D* spanwise length model. In addition, for 20° angle of attack, 2*D*, 3*D*, and 4*D* spanwise length models were used to validate the proposed method of estimating grid-independent fluctuating aerodynamic coefficients in Section 5. Table 2 shows system configurations of the PC cluster used in this study.

2.6. Definitions of aerodynamic coefficients

2.6.1. Pressure coefficients

Mean pressure coefficient, $\overline{C}_p$, and fluctuating pressure coefficient, C'_p, are respectively defined as follows:

$$\overline{C}_p = \frac{p - p_{ref}}{\frac{1}{2}\rho U^2}, C'_p = \sqrt{(C_p - \overline{C}_p)^2}. \quad (10)$$

where p_{ref} is the reference pressure located at mid point in spanwise direction of the lowest corner of the inlet boundary. Reference density ρ is 1.225 kg/m^3, and reference velocity U is

Table 1
Parameters used in this study.

Reynolds number UD/ν	10^4	
Non-dimensional time step size tU/D	0.04	
Spanwise length L	1*D*	6*D*
Curvature of the corner r	$D/100$	$D/100$
The number of mesh in spanwise direction N	10	60
The number of the mesh	175,000	1,050,000

Table 2
System configurations of the PC cluster used in this study.

CPU	Athlon 64 Processor 3200, 2.01 GHz
Number of nodes	20
Network	Gigabit Ethernet
OS	CentOS 4.0
CPU time for the case of $L = 6$D	125 h with 6 nodes

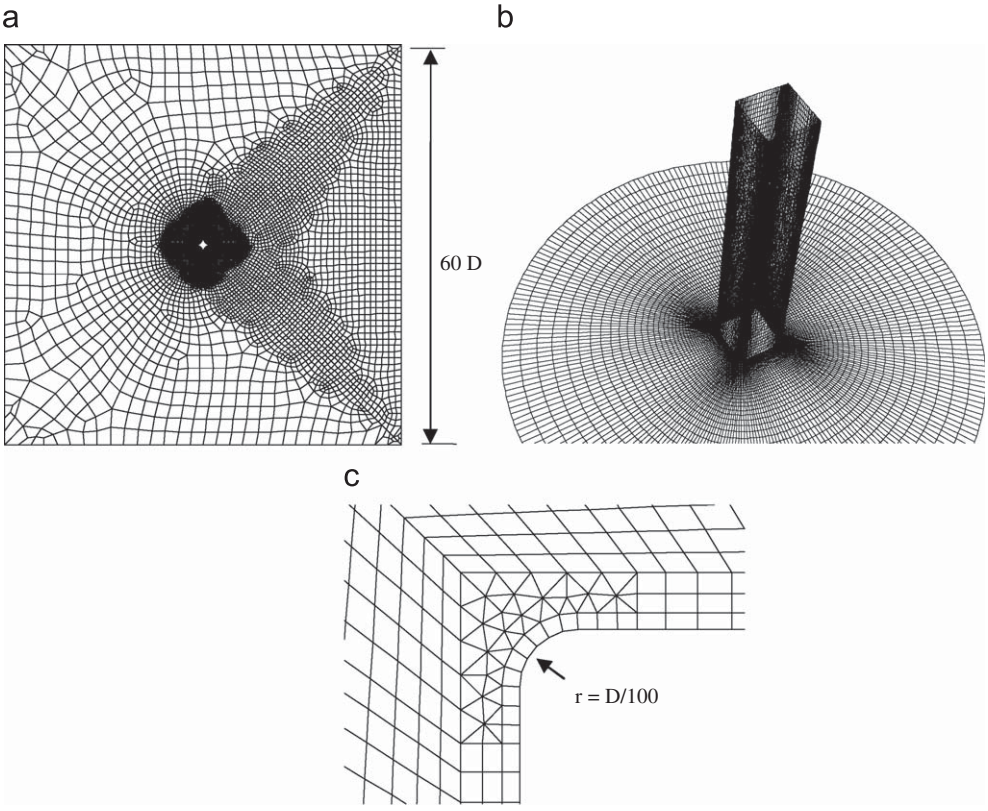

Fig. 1. Computational domain and mesh: (a) computational domain; (b) mesh near the prism; (c) mesh in the vicinity of the corner.

same as inflow velocity. A mean pressure coefficient is obtained by calculating time average over non-dimensional time, tU/D, from 100 to 600 at each cell, then average of the cells in spanwise direction was taken. Similarly, aerodynamic coefficients are obtained.

A stationary condition can be achieved by evaluating relative errors of mean drag coefficient and deviations of drag and lift coefficients, except for mean lift coefficient to avoid division by zero. The representative four angles of attack was simulated with 600 non-dimensional time period and the first 100 non-dimensional time data were removed to eliminate the transit data. The relative errors decrease with increase in non-dimensional time period. For 600 non-dimensional time period, the relative error of mean drag coefficient becomes less than 1% and those of deviations of drag and lift coefficients remain less than 3% for all cases.

2.6.2. Drag and lift coefficients

The definitions of aerodynamic forces and angle of attack are shown in Fig. 2. As shown in the figure, angle of attack is defined so that front surface of the square prism is normal to the wind direction for $\alpha = 0^\circ$, and clockwise direction denotes a positive angles of attack. Mean drag coefficient, C_D, mean lift coefficient, C_L, fluctuating drag coefficient, C_D, and fluctuating lift coefficient, C_L, are defined as follows.

$$C_D = \sum_i \overline{C}_{pi} A_i \cos\beta_i / A, \; C_L = \sum_i \overline{C}_{pi} A_i \sin\beta_i / A, \tag{11}$$

$$C'_D = \sqrt{\overline{\left(\sum_i (C_{pi} - \overline{C}_{pi}) A_i \cos\beta_i / A\right)^2}}, \; C'_L = \sqrt{\overline{\left(\sum_i (C_{pi} - \overline{C}_{pi}) A_i \sin\beta_i / A\right)^2}} \tag{12}$$

where A_i is the area of the ith cell surface. Reference area, A, is a product of D and L. β_i, is angle between normal to the surface of ith cell and wind direction. In this study, contribution of shear stresses, which is estimated less than 0.2% by test calculations, are ignored.

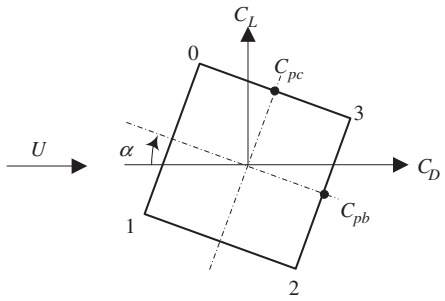

Fig. 2. Definitions of aerodynamic forces and angle of attack.

2.7. Experimental data for validation

In this study, experimental results of previous studies, Otsuki et al. (1978), Igarashi (1984), and Nishimura and Taniike (2000), are utilized for the validations purpose. Table 3 shows the descriptions of experiment conditions. Nishimura and Tannike's experiment was conducted in a well designed wind tunnel test, and satisfied the criteria of wind tunnel testing, such as high Reynolds number ($>10\,000$) and low blockage ($<5\%$). In addition, this reference provides highly qualified and comprehensive database, including not only mean and fluctuating aerodynamic coefficients but also surface pressure coefficients, Strouhal number, and power spectral.

3. Mean aerodynamics

Mean aerodynamic coefficients are the most important parameters in evaluation of dynamic response and galloping problems. This section shows performance and accuracy of the present numerical approach to simulate mean aerodynamics. First, mean aerodynamic coefficients for a range of angles of attack are predicted, and the effect of spanwise length is examined. Then, the mean pressures for the representative angles of attack are discussed to examine the relationship between mean aerodynamic forces and pressures. Finally, mean flow patterns are shown to clarify relationship between flow patterns and vortex formations in the wake.

3.1. Mean aerodynamic coefficients

Fig. 3 shows variations of mean drag and lift coefficients with angles of attack ranging from $\alpha = 0^\circ$ to 45°. The predicted mean drag coefficients moderately decrease with the increase in angle of attack from $\alpha = 0^\circ$ to 12°, and takes minimum value around $\alpha = 14^\circ$, and then increases with increase in α. The predicted mean lift coefficients show negative gradient between $\alpha = 0^\circ$ and 12° as observed in the experiments. From attack angle of $\alpha = 14^\circ$, mean lift coefficients increase with increase in α, and shows a flat curve in the range, larger than $\alpha = 30^\circ$. The acute change of mean lift coefficients around $\alpha = 14^\circ$, as observed in the experiments, is well captured by the present numerical approach.

To give a quantitative assessment of the results, the deviations of difference between simulations and experiments are examined. Assuming the experimental data by Otsuki as baseline, shown in Table 4, deviations of predictions are smaller than those of experiments by Otsuki and Nishimura, indicating that predicted mean aerodynamic coefficients are satisfactory.

Regarding the effect of spanwise length on mean drag and lift coefficients, no significant difference is observed for 1D and 6D, thus indicating that 1D spanwise length is fairly good for predicting mean aerodynamic forces. Further discussion on the effect of spanwise length on fluctuating aerodynamic coefficients will be presented in Section 4.1.

Table 3
Experimental conditions.

	Side dimension (cm)	Reynolds number	Turbulence intensity (%)	Blockage (%)
Nishimura and Taniike	6	4×10^4	0.1	1.5
Otsuki et al.	8	6.5×10^4–7.6×10^4	2	5.4
Igarashi	3	3.85×10^4–7.7×10^4	0.5	20

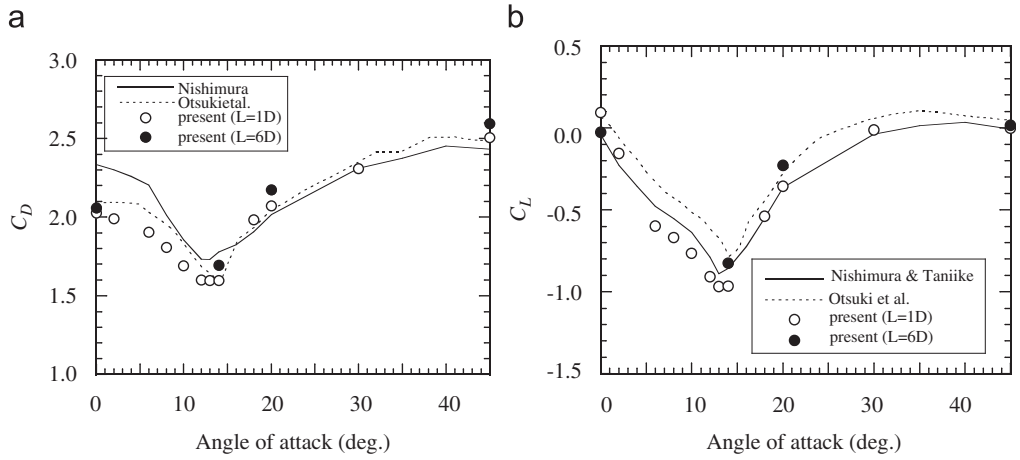

Fig. 3. Variations of mean drag and lift coefficients with angles of attack: (a) mean drag coefficients; (b) mean lift coefficients.

Table 4
The deviations of differences between simulations and experiments.

α	C_D		C_L	
	Difference between Otuski and predictions	Difference between Otuski and Nishimura	Difference between Otuski and predictions	Difference between Otuski and Nishimura
0	0.038	−0.238	0.075	0.092
14	−0.114	−0.199	0.041	0.072
20	−0.125	0.032	−0.043	0.093
45	−0.099	0.066	0.029	0.057
Deviation	0.076	0.156	0.050	0.017

3.2. Mean pressure coefficients

Variations of mean pressures coefficients along the peripheral of square prism with angles attack are shown in Fig. 4. The predicted pressure coefficients, at $\alpha = 0^\circ$, are negative on the upper and lower faces which corresponds to the flow pattern of perfect separation type. Pressure coefficients at the rear face ($x/B = 2$ to 3) are slightly overestimated compared to those obtained by the experiments. This is the reason why predicted drag coefficients are underestimated compared to Nishimura and Taniike (2000) as presented in the previous section.

Pressure recovery is observed in the vicinity of the trailing edge of lower face ($x/B = 1$ to 2) at $\alpha = 14^\circ$ where the intermittent reattachment of flow occurred as shown in Fig. 4(b). The predicted pressure coefficients of lower face before the pressure recovery region are smaller than those of $\alpha = 0^\circ$, and matches the experiment. In contrast to the pressure distributions on the lower face at $\alpha = 0^\circ$ and 14°, a peak in the pressure coefficients at $\alpha = 20^\circ$ can be observed near trailing edge of lower face as shown in Fig. 4(c). It indicates that reattachment of the shear layer occurred in this region continuously. Fig. 4(d) shows predicted pressure coefficients at $\alpha = 45^\circ$. Front face pressures are in good agreement with those from the experiment by Nishimura and Taniike (2000) while those of the rear face are slightly underestimated. This is why the mean drag coefficients at $\alpha = 45^\circ$ are slightly overestimated.

The difference of the forces between front and lower faces contributes negative lift force at $\alpha = 14^\circ$, and is larger than that at $\alpha = 20^\circ$, which results the minimum mean lift coefficient around $\alpha = 14^\circ$ as shown in Fig. 3(b). On the other hand, the difference of the forces between upper and lower faces at $\alpha = 0^\circ$ and those between front plus upper faces and lower plus rear faces at $\alpha = 45^\circ$ are canceled out, resulting the mean lift coefficients that are nearly zero as shown in Fig. 3(b).

Fig. 5 shows variations of mean pressure coefficients at the center of rear face with various angles of attack. Predicted mean pressure coefficients are smaller than those of experiments for $\alpha = 20^\circ$–45° range. The behavior of the shear layer and the corner curvature of the model might give rise to these underestimations. The corner curvature of the model used in present simulations is $D/100$, which is the same as that utilized by Tamura et al. (1990). However, no information about the corner curvature of experimental model shown in Table 3 is available, which may result in discrepancies between experiments and simulations.

3.3. Flow patterns

Fig. 6 shows mean streamlines for representative angles of attack. Shear layer forms a perfect separation type flow at $\alpha = 0^\circ$ where no reattachment of flow to the lower face is observed, and two large vortexes are formed in the wake as shown in Fig. 6(a). At $\alpha = 14^\circ$, separated flow at front edge intermittently reattaches to the lower face in the vicinity of trailing edge, and a large single vortex is formed in the wake region as shown in Fig. 6(b). The shear layer for $\alpha = 20^\circ$ case clearly shows reattachment near the trailing edge region as shown in Fig. 6(c). The area of separation bubble, generated at front edge of the lower face, becomes smaller compared to that at $\alpha = 14^\circ$, and single vortex is also formed in the wake region. This implies that the frequencies of vortex shedding at $\alpha = 14^\circ$ and 20° might be different from those obtained at $\alpha = 0^\circ$ and 45°.

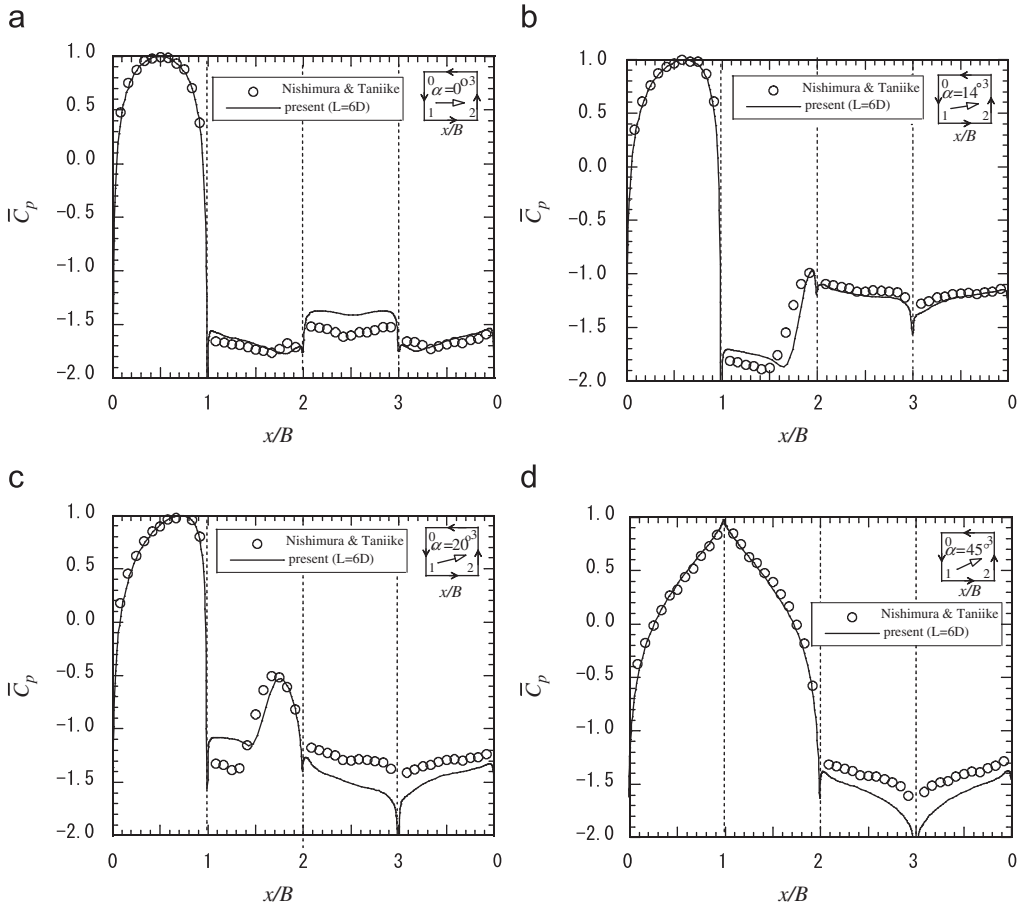

Fig. 4. Variations of mean pressure coefficients with angles of attack: (a) $\alpha = 0^\circ$; (b) $\alpha = 14^\circ$; (c) $\alpha = 20^\circ$; (d) $\alpha = 45^\circ$.

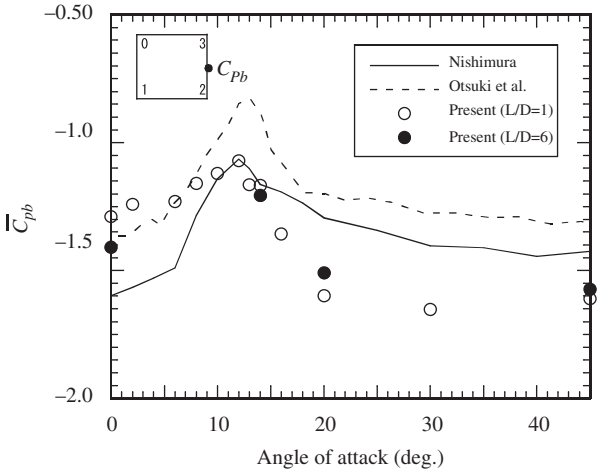

Fig. 5. Variations of mean pressure coefficients at the center of rear face with angle of attack.

4. Fluctuating aerodynamics

Fluctuating aerodynamics is important for vortex induced vibration and aeroacoustics problems. Firstly, fluctuating aerodynamic coefficients with 1*D* and 6*D* spanwise length models for various angles of attack are investigated. Then, fluctuating pressure coefficients at rear and upper faces are presented. And distribution of fluctuating pressure coefficients at representative angles of attack are compared with experiments. Finally, Strouhal numbers are sought to verify the dominant frequencies of vortex shedding against the experimental ones. Power spectral densities of fluctuating aerodynamic coefficients are obtained to identify frequency of vortex shedding in the wake region. The relationship between frequency of vortex shedding and mean flow pattern is investigated.

4.1. Fluctuating aerodynamic coefficients

Fig. 7 shows variations of fluctuating drag and lift coefficients with angles of attack. Predicted fluctuating drag coefficients of 6*D* span length models show good agreement with the Nishimura and Taniike (2000), while those of 1*D* models are overestimated for angle of attack ranging from $\alpha = 14^\circ$ to 45°. Predicted fluctuating lift coefficients decrease with increase in the angle from $\alpha = 0^\circ$ to 10°. This tendency matches that of the experiments by Nishimura and Taniike (2000) for angles of attack larger than $\alpha = 10^\circ$. The results with 6*D* spanwise length models are closer to the experiments compared to those of 1*D* model, indicating that spanwise length significantly influences the accuracy of fluctuating aerodynamic coefficients. Although assuming a sufficient spanwise length of model can obtain a grid-independent solution, huge amount of computational costs are required. Therefore, spanwise length issue becomes important for accurate prediction of fluctuating aerodynamics, and will be discussed in Section 5.

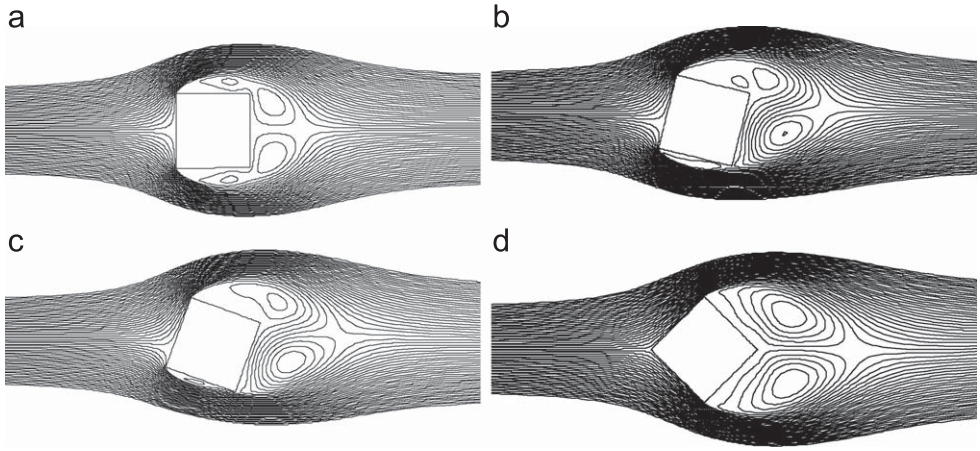

Fig. 6. Variations of mean streamlines with angles of attack: (a) $\alpha = 0^\circ$; (b) $\alpha = 14^\circ$; (c) $\alpha = 20^\circ$; (d) $\alpha = 45^\circ$.

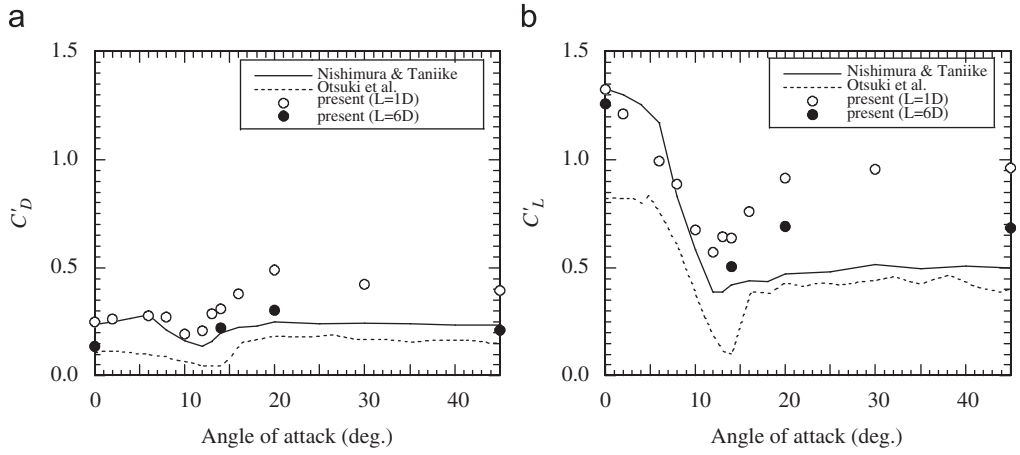

Fig. 7. Variations of fluctuating coefficients with angles of attack: (a) fluctuating drag coefficients; (b) fluctuating lift coefficients.

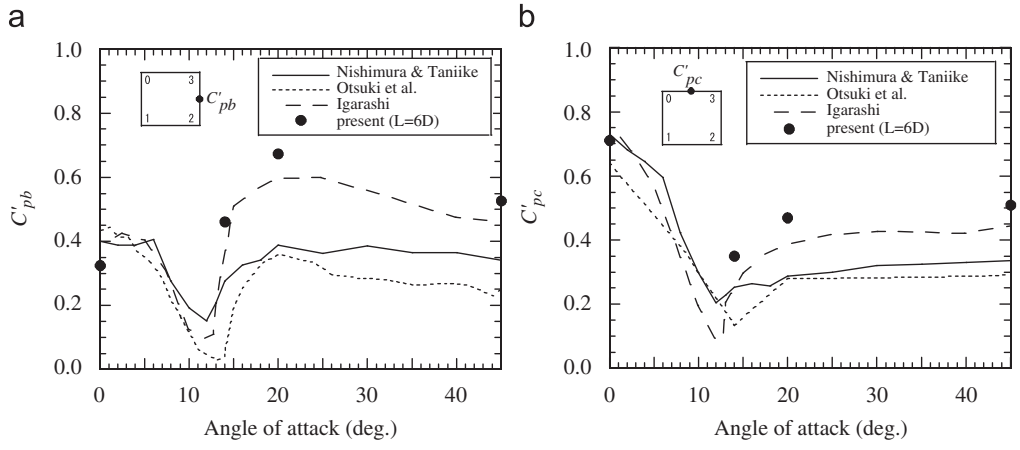

Fig. 8. Variations of fluctuating pressure coefficients with angles of attack: (a) at rear face center; (b) at upper face center.

4.2. *Fluctuating pressure coefficients*

Variations of fluctuating pressure coefficients at rear and upper face centers with change in angles of attack are shown in Fig. 8(a) and (b), and good agreement is found with Igarashi (1984) for all angles of attack. However, these are overestimated compared to the experiments by Nishimura and Taniike (2000) and Otsuki et al. (1978) at angles larger than $\alpha = 20^\circ$. These discrepancies may be caused by corner curvature of models and turbulence of the incoming inflow.

Fig. 9 shows fluctuating pressure coefficients normalized by the pressure coefficient of upper face center for the comparison. The predicted fluctuating pressure coefficients are in good agreement with the Nishimura and Taniike (2000) at $\alpha = 0^\circ$ as shown in Fig. 9(a), except for those at trailing edge of the upper and the lower surfaces where reversed flow reattaches

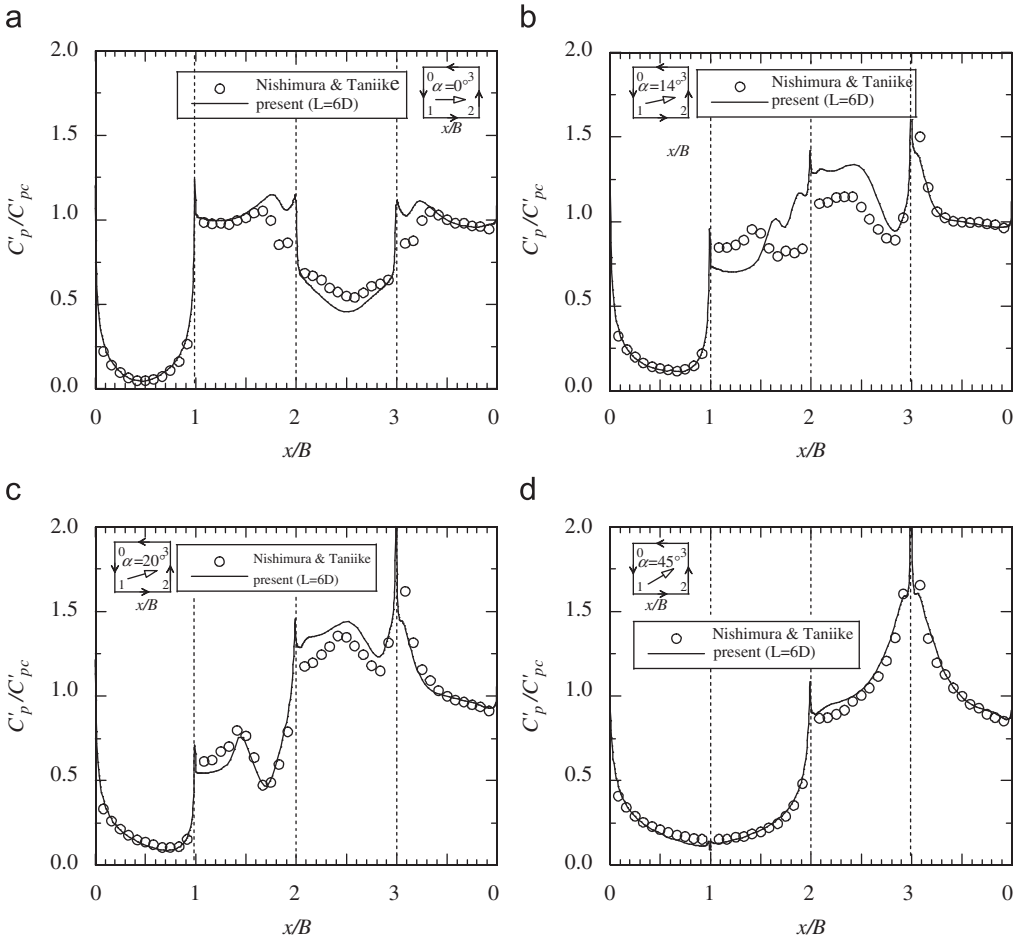

Fig. 9. Fluctuating pressure coefficients normalized by the pressure coefficient at upper face center: (a) $\alpha = 0^\circ$; (b) $\alpha = 14^\circ$; (c) $\alpha = 20^\circ$; (d) $\alpha = 45^\circ$.

intermittently. The difference between prediction and experiment appear near corners 1 and 2 at $\alpha = 14^\circ$. This flow pattern might be sensitive to the angle of attack around $\alpha = 14^\circ$ and small difference in angle could cause significant change of fluctuating pressure. At $\alpha = 20^\circ$, predicted fluctuating pressure coefficients at the lower face as shown in Fig. 9(c), shows a local maximum near center of lower face and takes local minimum value in the downstream region where reattachments are supposed to occur continuously. Although the predicted pressure coefficients at $\alpha = 20^\circ$ are slightly overestimated on the rear face, the predictions at $\alpha = 45^\circ$ are found in good agreement with experiment on all faces.

4.3. Power spectral of fluctuating aerodynamic forces

It is well known that frequency of vortex shedding of a perfect separation type flow is closely related to interference between separation shear layer and wake, whereas frequency of vortex shedding of a reattachment type flow is determined by interference between separation shear layer and trailing edge (Igarashi, 1984).

Fig. 10 shows variation of Strouhal number, S_t, with angles of attack, which is defined by $f_s D/U$ and f_s is a dominant frequency of fluctuating lift force. The predicted Strouhal numbers are qualitatively in good agreement with experiments for both types of flows, that is, perfect separation and reattachment types. The simulated results capture the acute change at $\alpha = 14^\circ$, where the flow pattern is sensitive to the angle of attack and small difference of angle could cause significant difference in fluctuating pressure as discussed in previous section. This indicates that the numerical simulation can quantitatively predict vortex shedding of square prism for various angles of attack.

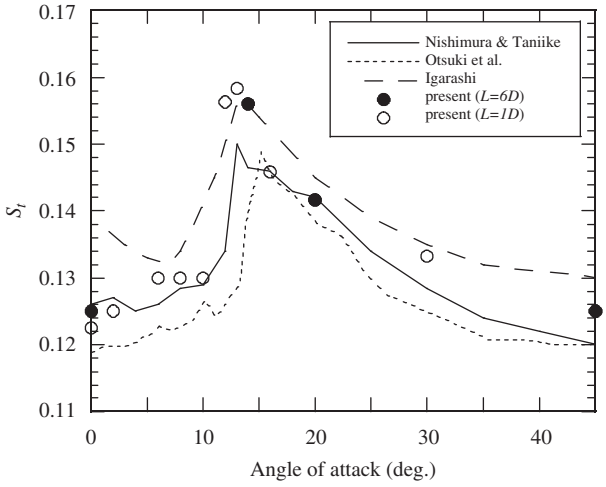

Fig. 10. Variation of Strouhal number with angles of attack.

Normalized power spectral densities of fluctuating aerodynamic forces have close relationship with vortex formation in the

wake. As shown in Fig. 11(a), (b), (g), and (h), the primary frequencies of fluctuating drag forces are two times higher than corresponding fluctuating lift forces at $\alpha = 0^\circ$ and 45°, and show fairly good agreement with Nishimura and Taniike (2000), denoted by open circle, and Nishimura (2001). However, there is a moderate peak for predicted drag that does not exist in the measured fluctuating drag in the low frequency range for case of $\alpha = 0^\circ$. Pressure with the vortex may be reflected at the side boundaries. Alternating vortex shedding from upper and lower side of the square prism is associated with the primary frequency of drag that is twice the primary frequency of lift. The drag force has one maximum and one minimum during the growth and shedding of each vortex, while the sign of the lift force changes when vortex is shedding from upper or lower side of square prism. At $\alpha = 14^\circ$ and 20°, the primary frequencies of fluctuating drag forces are coincident with those of fluctuating lift forces as shown in Fig. 11(c)–(f). The change of the primary frequency is associated with the transition of the flow pattern in the wake region, in which the pattern of vortex shedding has changed from alternate vortex shedding to a single large vortex shedding as shown in Fig. 6(b) and (c). Though the predicted spectral power densities of fluctuating aerodynamic forces are fairly in good agreement with

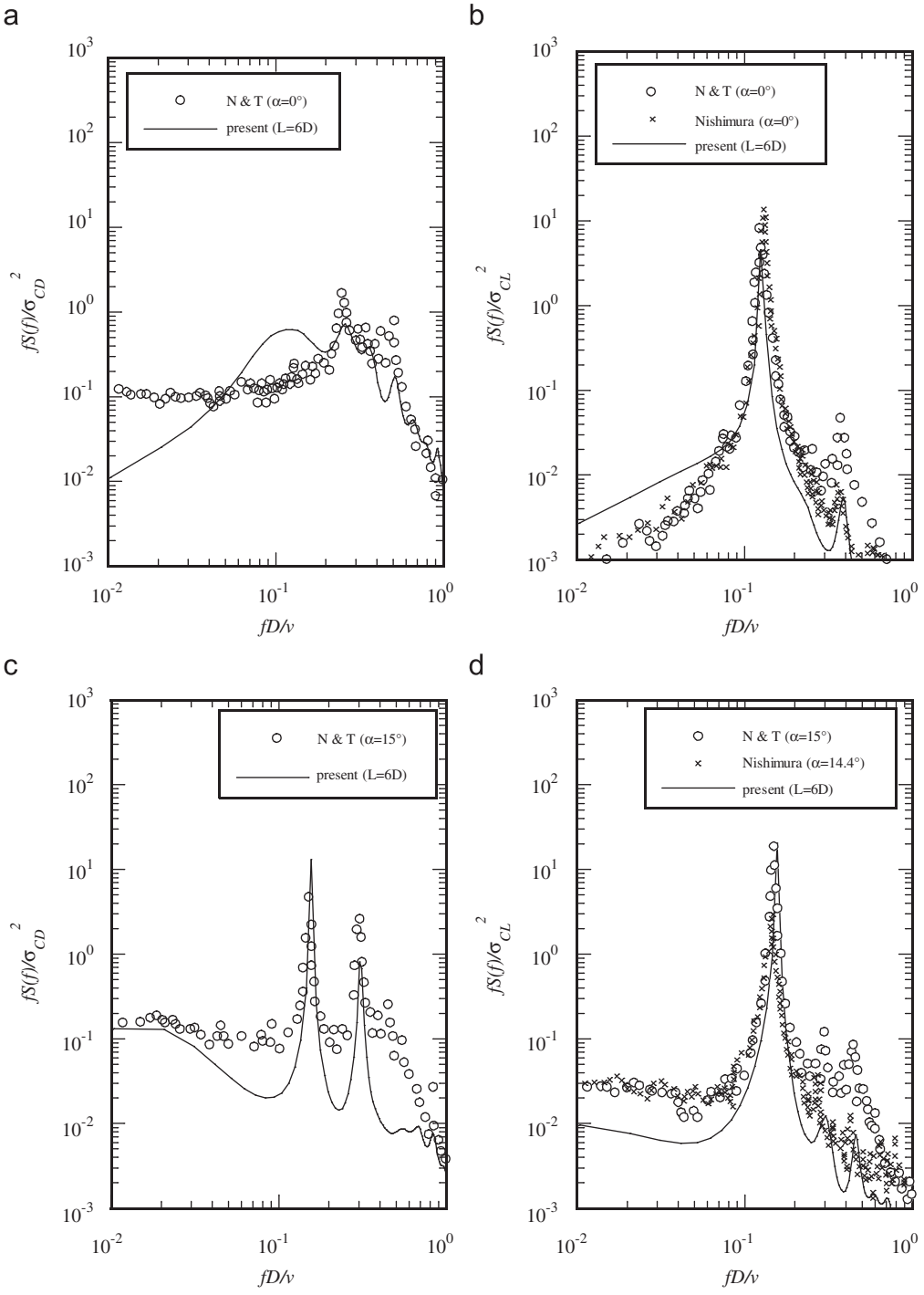

Fig. 11. Normalized power spectral densities of fluctuating aerodynamic forces: (a) drag coefficients at $\alpha = 0^\circ$; (b) lift coefficients at $\alpha = 0^\circ$; (c) drag coefficients $\alpha = 14^\circ$; (d) lift coefficients at $\alpha = 14^\circ$; (e) drag coefficients at $\alpha = 20^\circ$; (f) lift coefficients at $\alpha = 20^\circ$; (g) drag coefficients at $\alpha = 45^\circ$; (h) lift coefficient at $\alpha = 45^\circ$.

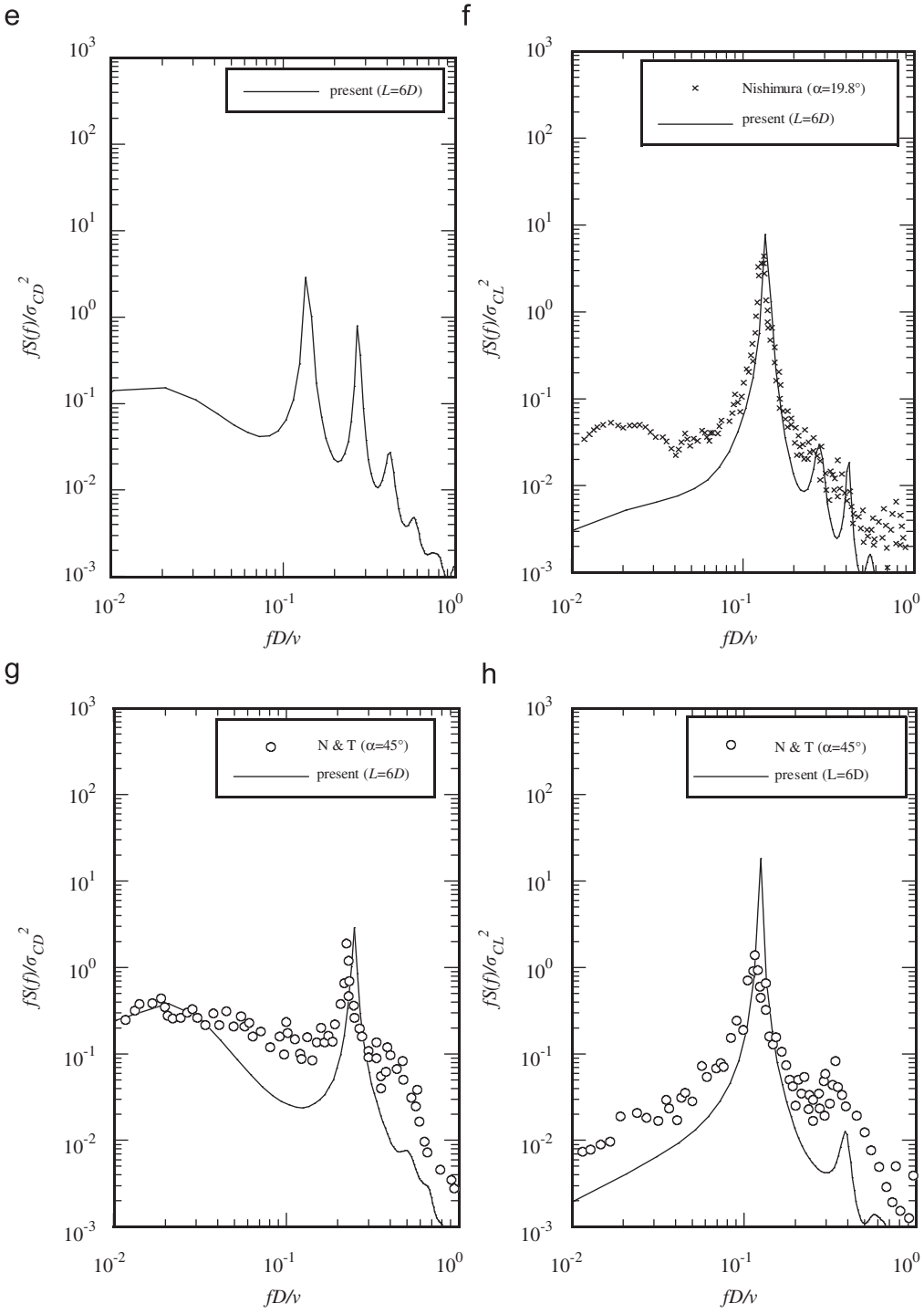

Fig. 11. (*Continued*)

the experiments, small discrepancies are observed in low frequency region. Further study is necessary to resolve this issue.

5. An estimation of grid-independent fluctuating aerodynamic coefficients

Spanwise length affects the accuracy of fluctuating aerodynamic coefficients as mentioned in Section 4. The sufficient spanwise length is necessary to reduce the errors. On the other hand, computation costs increases considerably when longer spanwise length models are used.

In this section, we propose a practical method to estimate grid-independent fluctuating aerodynamic force coefficients using a systematic procedure, which would significantly save calculation time and memory.

Fig. 12 shows the variation of fluctuating aerodynamic coefficients and estimated errors for spanwise length factor defined below. Errors of the predictions monotonically decrease as longer spanwise length models were used. Let ϕ_γ is an

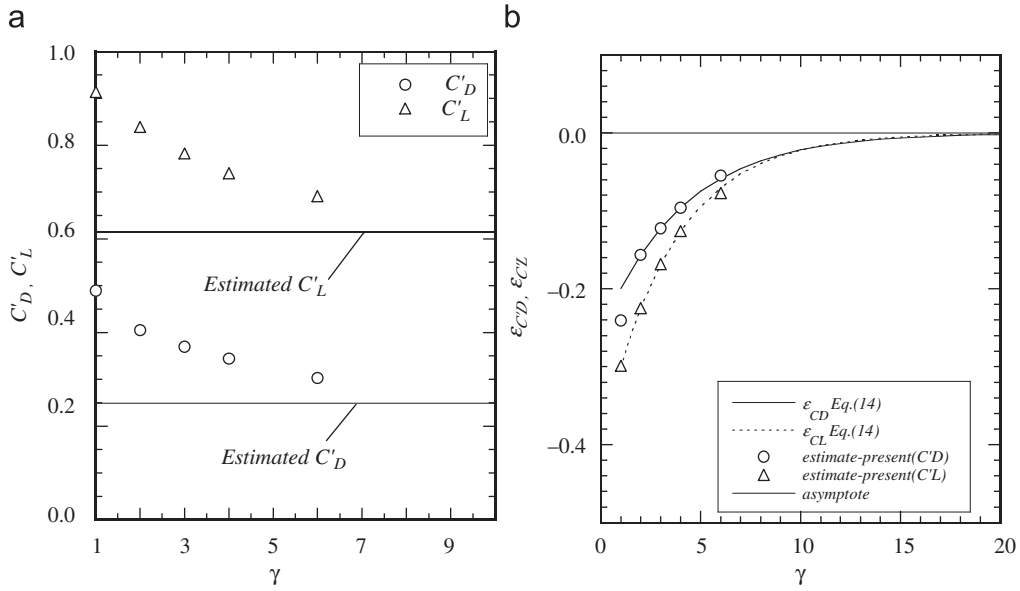

Fig. 12. Variation of fluctuating aerodynamic coefficients and estimated errors with spanwise length factors: (a) fluctuating aerodynamic coefficients; (b) estimated errors.

Table 5
Evaluations of cost performance.

	(a) Proposed method ($L = 2D$, $3D$, $4D$)	(b) Conventional approach ($L = 20D$)	Cost performance (b)/(a)	Network
Case 1	9(2, 3, 4)	20	2.2	Ideal condition
Case 2	10.6(2.2, 3.5, 4.9)	42.4	4.0	Gigabit Ethernet

aerodynamic coefficient obtained by using a spanwise length, $L = \gamma D$, where γ is the spanwise length factor that is an arbitrary positive integer other than zero. By defining ε_γ as an error for the responding spanwise length model, a grid-independent aerodynamic coefficient, Φ, is expressed as:

$$\Phi = \phi_\gamma + \varepsilon_\gamma, \tag{13}$$

Suppose that if predicted error monotony decreases as γ increases, the prediction error can be approximated by an exponential function.

$$\varepsilon_\gamma = \beta e^{-c\gamma}, \tag{14}$$

where c is a decay factor and β is a proportionality coefficient. The grid-independent aerodynamic coefficients can be estimated by:

$$\Phi = \phi_\gamma + \beta e^{-c\gamma}, \tag{15}$$

Since the grid-independent aerodynamic coefficients may be expressed as:

$$\Phi = \phi_\gamma + \beta e^{-c\gamma} = \phi_{\gamma+1} + \beta e^{-c(\gamma+1)} = \phi_{\gamma+2} + \beta e^{-c(\gamma+2)}, \tag{16}$$

the β and c may be estimated as follows:

$$\beta = \frac{\phi_{\gamma+1} - \phi_\gamma}{1 - e^{-c}} e^{c\gamma}, \tag{17}$$

$$c = \ln \frac{\phi_{\gamma+1} - \phi_\gamma}{\phi_{\gamma+2} - \phi_{\gamma+1}}. \tag{18}$$

Similar approach was used in Richardson extrapolation in which discretization errors of partial differential equations are estimated using power function (Richardson, 1910; Roache, 1994). The reason why we use exponential function rather than power function employed by Richardson (1910) is that the longer spanwise length of models, the exponentially smaller the turbulence correlation factor (Wooton and Scruton, 1971).

Estimated fluctuating aerodynamic coefficients for shorter spanwise length models of $2D$, $3D$, and $4D$ are used to verify the proposed method as shown in Fig. 12(a). It is noticed that fluctuating aerodynamic coefficients are plotted closer to the asymptotes as the spanwise length of model increases. Fig. 12(b) shows variation of estimated errors with spanwise length factor. Estimated errors decrease with increase in spanwise length factor. Accuracy obtained by the proposed method is of the same level as that is obtained by conventional approach in which the spanwise length of $20D$ was used, as shown in Fig. 12(b).

When parallel computers and distributed memory were used for speeding up the simulation, efficiency of parallel computing is usually reduced with increase in number of processors for a given mesh. Total efficiency, E_n^{tot}, can be expressed as:

$$E_n^{tot} = E_n^{mun} E_n^{par} E_n^{lb}, \tag{19}$$

where, E_n^{num} is numerical efficiency, E_n^{par} is parallel efficiency, E_n^{lb} is load balancing efficiency, as shown by Ferziger and Peric (2002).

The cost performance of a PC cluster with Gigabit Ethernet used in this study is evaluated by assuming that the numerical efficiency and load balancing efficiency are 1, because a multigrid solver is used and the solution domain is subdivided into the same size.

Table 5 shows the cost performance of the proposed method. Case 1 shows the cost for ideal condition of the network and case 2 shows that of the PC cluster. The cost of the proposed method is 1/4 of the conventional approach and the speedup ratio is about 8.7 when Gigabit Ethernet Network is used. It should be noted that the efficiency of parallel computing differs from system to

system, so the cost performance evaluation should be performed for each system.

6. Conclusions

Aerodynamic characteristics of square prism in a uniform flow with various angles of attack have been investigated using LES model. Following summarizes the findings and conclusions of this study:

(1) The predicted mean aerodynamic coefficients for various angles of attack show good agreements with experiments and the peak near the 14° attack angle is well captured. Mean pressure coefficients are in good agreement with experiments and mean flow patterns closely related to vortex formations in the wake are well revealed.
(2) The predicted fluctuating aerodynamic coefficients as well as the fluctuating pressure coefficients for various angles of attack are compared with experiments and a satisfactory agreement is obtained. The predicted Strouhal numbers also agree with the experiments and well capture the peak around $\alpha = 14^{\circ}$. The primary and secondary frequencies in the predicted power spectral densities of fluctuating aerodynamic forces coincide with the experiments and match the vortex formations in the wake region.
(3) The spanwise length of computational domain slightly influences mean aerodynamic coefficients whereas it gives strong impact on fluctuating aerodynamic coefficients. It is found that the spanwise length of $1D$ is practically enough for the predictions of mean values.
(4) A method for estimating grid-independent fluctuating aerodynamic coefficients is proposed to improve accuracy of the predicted fluctuation obtained by using smaller spanwise length, which is in turn reduces cost and memory for the simulations. It is noticed that a numerical model with spanwise length of $4D$ is sufficient for the proposed method, whereas $20D$ is ideally required for the conventional approach.

Acknowledgment

Authors would like to thank Dr. Akihiro Nishimura to provide his valuable experiments data for this study.

References

Bearman, P.W., Obasaju, E.D., 1982. An experimental study of pressure fluctuations on fixed and oscillating square-section cylinders. J. Fluid Mech. 119, 297–321.
Bosch, G., Rodi, W., 1998. Simulation of vortex shedding past a square cylinder with different turbulence models. Int. J. Numer. Meth. Fluids 28, 601–616.
Curle, N., 1955. The influence of solid boundaries upon aerodynamic sound. Proc. R. Soc. A 231, 505–514.
Ferziger, J., Peric, M., 2002. Computational Method for Fluid Dynamics, third ed. Springer, Berlin.
Hayashi, K., Ohya, Y., 2000. A numerical study of the flow around a rectangular cylinder with critical depth. In: Proceedings of 16th National Symposium on Wind Engineering, pp. 179–184 (in Japanese).
Hirano, H., Maruoka, A., Watanabe, S., 2002. Calculations of aerodynamic properties of rectangular cylinder with slenderness ratio of 2:1 under various angles of attack. J. Struct. Eng. 48A, 971–978 (in Japanese).
Igarashi, T., 1984. Characteristics of the flow around a square prism. Bull. JSME 27, 231 1858–1865.
Kato, C., Iida, A., Ikegawa, M., 1993. Numerical simulation of aerodynamic sound radiated from low mach number turbulent wakes. AIAA 93-0145.
Lighthill, M.J., 1952. On sound generated aerodynamically; I general theory. Proc. R. Soc. A 211, 564–587.
Ma, X., Karamanos, G.S., Karniadakis, G.E., 2000. Dynamics and low-dimensionality of a turbulent near wake. J. Fluid Mech. 410, 29–65.
Mizota, T., Okajima, A., 1981. Experimental studies of the mean flows around rectangular prisms. Trans. Jpn. Soc. Civ. Eng. 13, 79–81.
Nishimura, A., Taniike, Y., 2000. Fluctuating wind forces of a stationary two dim. square prism. In: Proceedings of 16th National Symposium on Wind Engineering, pp. 255–260 (in Japanese).
Nishimura, A., 2001. Fundamental study of bluff body aerodynamics. Ph.D. Thesis, Kyoto University, in Japanese.
Ohya, A., Washizu, K., Fujii, K., Otsuki, Y., 1980. Wind tunnel experiments on aerodynamic forces and pressure distributions of rectangular cylinders in a uniform flow (part 2). Proc. Nat. Symp. Wind Eng. , 153–160 (in Japanese).
Otsuki, Y., Fujii, K., Washizu, K., Ohya, A., 1978. Wind tunnel experiments on aerodynamic forces and pressure distributions of rectangular cylinders in a uniform flow. In: Proceedings of the Fifth Symposium on Wind Effects on Structures, pp. 169–176 (in Japanese).
Parkinson, G.V., 1971. Wind-induced instability of structure. Philos. Trans. R. Soc. London, Ser. A 269, 395–409.
Richardson, L.F., 1910. The approximate arithmetical solution by finite differences of physical problems involving differential equations with an application to the stresses in a masonry dam. Trans. R. Soc. London, Ser. A 210, 307–357.
Roache, P.J., 1994. Perspective: a method for uniform reporting of grid refinement studies. ASME J. Fluid Eng. 116, 405–413.
Rodi, W., 1997. Comparison of LES and RANS calculations of the flow around bluff bodies. J. Wind Eng. Ind. Aerodyn. 69–71, 55–75.
Shimada, K., Ishihara, T., 2001. Application of a modified k–ε model to the prediction of aerodynamic characteristics of rectangular cross-section cylinders. J. fluids Struc. 16 (4), 465–485.
Shimizu, M., Ishihara, T., Phuc, V., 2004. A wind tunnel study on aerodynamic characteristics of ice accreted transmission lines. In: Fifth International Colloquim on Bluff Body Aerodynamics and Applications, Summary Papers, pp. 369–372.
Smagorinsky, J., 1963. General circulation experiments with the primitive equations. I. The basic experiment. Month. Wea. Rev. 91, 99–164.
Tamura, T., Ohta, I., Kuwahara, K., 1990. On the reliability of two-dimensional simulation for unsteady flows around a cylinder-type. J. Wind Eng. Ind. Aerodyn. 35, 275–298.
Taylor, I., Vezza, M., 1999. Calculation of the flow field around a square section cylinder undergoing forced transverse oscillations using a discrete vortex. J. Wind Eng. Ind. Aerodyn. 82, 271–291.
Vickery, B.J., 1966. Fluctuating lift and drag on a long cylinder of square cross-section in a smooth and in a turbulent stream. J. Fluid Mech. 25, 481–494.
Wooton, L.R., Scruton, C., 1971. Aerodynamic stability. The modern design of wind-sensitive structures, CIRIA seminar.